The Climate Signal in Regional Moisture Fluxes: A Comparison of Three Global Data Assimilation Products

WEI MIN*

University Space Research Association, Seabrook, Maryland

SIEGFRIED SCHUBERT

Data Assimilation Office, NASA/Goddard Space Flight Center, Greenbelt, Maryland

(Manuscript received 30 September 1996, in final form 28 January 1997)

ABSTRACT

This study assesses the quality of estimates of climate variability in moisture flux and convergence from three assimilated datasets: two are reanalysis products generated at the Goddard Data Assimilation Office and the National Centers for Environmental Prediction–National Center for Atmospheric Research, and the third consists of the operational analyses generated at the European Centre for Medium-Range Weather Forecasts (ECMWF). The regions under study (the United States Great Plains, the Indian monsoon region, and Argentina east of the Andes) are characterized by frequent low-level jets and other interannual low-level wind variations tied to the large-scale flow. While the emphasis is on the reanalysis products, the comparison with the operational product is provided to help assess the improvements gained from a fixed analysis system.

All three analyses capture the main moisture flux anomalies associated with selected extreme climate (drought and flood) events during the period 1985–93. The correspondence is strongest over the Great Plains and weakest over the Indian monsoon region reflecting differences in the observational coverage. For the reanalysis products, the uncertainties in the lower tropospheric winds is by far the dominant source of the discrepancies in the moisture flux anomalies in the middle latitude regions. Only in the Indian Monsoon region, where interannual variability in the low-level winds is comparatively small, does the moisture bias play a substantial role. In contrast, the comparisons with the operational product show differences in moisture that are comparable to the differences in the wind in all three regions.

Compared with the fluxes, the anomalous moisture convergences show substantially larger differences among the three products. The best agreement occurs over the Great Plains region where all three products show vertically integrated moisture convergence during the floods and divergence during the drought with differences in magnitude of about 25%. The reanalysis products, in particular, show good agreement in depicting the different roles of the mean flow and transients during the flood and drought periods. Differences between the three products in the other two regions exceed 100% reflecting differences in the low-level jets and the large-scale circulation patterns. The operational product tends to have locally larger amplitude convergence fields, which average out in area-mean budgets: this appears to be at least in part due to errors in the surface pressure fields and aliasing from the higher resolution of the original ECMWF fields.

On average, the reanalysis products show higher coherence with each other than with the operational product in the estimates of interannual variability. This result is less clear in the Indian monsoon region where differences in the input observations appear to be an important factor. The agreement in the anomalous convergence patterns is, however, still rather poor even over relatively data-dense regions such as the United States Great Plains. These differences are attributed to deficiencies in the assimilating general circulation model's representations of the planetary boundary layer and orography, and a global observing system incapable of resolving the highly confined low-level winds associated with the climate anomalies.

1. Introduction

Understanding the mechanisms of climate change requires accurate estimates of the hydrological cycle and its linkages on both regional and global scales. Early estimates of atmospheric moisture fluxes (e.g., Benton and Estoque 1954; Rasmusson 1967 and 1968; Rosen et al. 1979; Peixoto and Oort 1983) helped to highlight both the importance of the low-level (planetary boundary layer) winds for determining the moisture transport, and the inadequacy of the rawindsonde network for obtaining accurate estimates of water vapor flux convergence. The latter is a key quantity that, if sufficiently accurate, offers the opportunity to estimate a number of other difficult to observe hydrological parameters. For example, Rasmusson (1968) showed how evaporation can be estimated over North America as a residual of

* Current affiliation: General Science Corporation, Laurel, Maryland.

Corresponding author address: Dr. Wei Min, Code 910.3, Data Assimilation Office, NASA/Goddard Space Flight Center, Greenbelt, MD 20771.
E-mail: min@dao.gsfc.nasa.gov

the atmospheric water budget provided estimates of precipitation are available. Furthermore, surface–subsurface water storage changes can be estimated if streamflow is known. While promising, that study pointed to deficiencies in the atmospheric station data that limits the application to regions with a high density station network and requires considerable spatial averaging of the budget equations.

The limitations of the station network involve not only insufficient spatial sampling but also insufficient resolution in time. For example, Rasmusson (1967) studied the atmospheric water vapor transport over North America and found a substantial diurnal cycle, which he linked to the southerly low-level jet (LLJ) over the Great Plains. The jet maximum typically occurs in the early morning hours, which fall between the 0000 UTC and 1200 UTC station observations. The time-sampling problem combined with the small vertical extent of the Great Plains LLJ (e.g., Bonner 1968; Bonner and Paegle 1970) makes it a difficult phenomenon to study from the station observations alone. The Great Plains region is in fact only one of a number of regions throughout the world that are characterized by strong highly confined low-level wind maxima (see, e.g., Paegle 1984; Stensrud 1996).

In recent years new estimates of the moisture fluxes have been obtained from model simulations or from a combination of model and observational estimates through the process of data assimilation. For example, Helfand and Schubert (1995) studied the Great Plains LLJ and its contribution to the moisture budget of the United States employing general circulation model (GCM) simulations. They concluded that the LLJ plays a key role in the moisture budget by transporting about one-third of all the moisture that enters the continental United States. Roads et al. (1994) conducted a comprehensive study of the United States hydrological cycle employing observations and the National Centers for Environmental Prediction (NCEP, formerly known as the National Meteorological Center) operational analyses. While the results were generally encouraging, significant discrepancies existed between surface water estimates from residual atmospheric moisture flux calculations and measurements of pan evaporation. Matsuyama et al. (1994) studied the moisture budget in the vicinity of the Congo River Basin in Africa by using the operational analysis of the European Centre for Medium-Range Weather Forecasts (ECMWF). Matsuyama (1992) compared the atmospheric flux convergence of water vapor to river discharge in the Amazon Basin. He concluded that atmospheric inflow needs to be adjusted by a constant scale factor to match river outflow. Higgins et al. (1996) studied the moisture budget for May over the central United States using a 5-yr subset of the the National Centers for Environmental Prediction–National Center for Atmospheric Research (NCEP–NCAR) and the National Aeronautics and Space Administration/Goddard Data Assimilation Office (NASA/DAO) reanalysis datasets. They found that both reanalyses overestimate the climatological mean precipitation rates by nearly a factor of 2 over the southeastern United States, and that there are substantial differences in the mean moisture divergence fields. In another study employing the same NCEP–NCAR and NASA/DAO datasets, Mo and Higgins (1996) found that the large-scale moisture transport is in general agreement in the two reanalyses despite regional differences, and that the discrepancies of moisture transport in the Tropics are largely due to the divergent wind. Wang and Paegle (1996) compared the moisture flux and moisture convergence over North and South America continents using NCEP, U.K. Meteorological Office (UMKO), and ECMWF operational analyses. They concluded that the differences in the regional moisture flux among these datasets were principally due to the uncertainty of the wind fields and, in particular, the low-level jets.

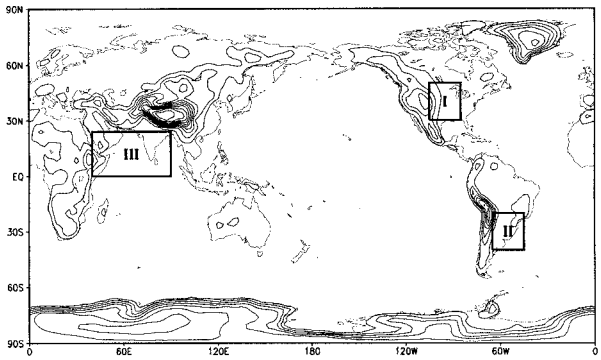

FIG. 1. Computational domains (boxes). Region I: the United States Great Plains, region II: Argentina east of the Andes, and region III: the Indian monsoon region. Contours show the orography used in the DAO assimilation system. Contour interval is 500 m.

While four-dimensional data assimilation makes it possible, in principle, to completely evaluate the hydrological cycle of the earth–atmosphere system, the above studies have shown that substantial bias exists in the assimilated data. Nevertheless, the assimilated data may provide reasonable estimates of the deviations (or anomalies) from the climate means (see, e.g., Schubert et al. 1995). The purpose of this study is to examine the quality of the interannual variability of the moisture fluxes obtained from global assimilated data products. By focusing on interannual variability, we hope to exploit what is perhaps the key strength of the recently completed reanalysis products: the absence of artificial climate signals resulting from system changes often found in operational analyses. We examine in some detail the quality of the summer climate signals in the moisture transport and convergence for several key regions (region I: the United States Great Plains; region II: Argentina east of the Andes; and region III: the Indian monsoon region, see Fig. 1). These regions are characterized by strong LLJs and other low-level wind

fluctuations tied to changes in the large-scale circulation.

The datasets consist of the reanalyses produced by the NASA/DAO (Schubert et al. 1993), the NCEP–NCAR (Kalnay et al. 1996), and the operational analyses produced at ECMWF. While the focus is on the reanalysis products, the comparison with the operational product provides some measure of the improvements gained from employing an unvarying analysis system. As described in section 2, these systems differ in the general circulation model employed, the assimilation techniques, and the input datasets. The emphasis is on periods of drought and flooding. These consist of June 1988 and July 1993 for the U.S. Great Plains, December 1985 and February 1992 for the South American region, and May 1987 and May 1988 for the Indian monsoon region. During July 1993, the United States midwest was under severe flooding conditions while much of the central and eastern United Sates suffered severe heat waves and drought conditions in June 1988. During December of 1985, southeastern Brazil experienced drought conditions, while during February 1992 southern Brazil, northern Argentina, and northern Uruguay experienced heavy rains. The Indian monsoon region experienced a drought during the summer of 1987 and a good monsoon during 1988. The month of May was chosen to highlight the interannual differences in the monsoon onset.

Section 2 summarizes the main components of the assimilation systems at the three data centers and the major differences among these systems. Section 3 compares the vertically integrated moisture fluxes and moisture convergence over the three key regions. The sources of the uncertainty in the moisture flux and flux convergence is examined in section 4. The summary and conclusions are given in section 5.

2. The data and data processing

The DAO datasets are a subset of a multiyear reanalysis with a nonvarying assimilation system (Schubert et al. 1993), which consists of version 1 of the Goddard Earth Observing System (GEOS-1) general circulation model (GCM; Takacs et al. 1994) and a three-dimensional multivariate optimal interpolation (OI) scheme (Pfaendtner et al. 1995). The analysis is carried out on 14 standard pressure levels extending from 1000 to 20 mb. The GEOS-1 GCM is a gridpoint model employing the Aries–GEOS dynamical core described in Suarez and Takacs (1995). For the reanalysis, the GCM was run at a horizontal resolution of 2° lat $\times$ 2.5° long and with 20 sigma levels in the vertical (top at 10 mb). The assimilation system does not include an initialization scheme and relies on the damping properties of a Matsuno time-differencing scheme to control initial imbalances generated by the insertion of observations. However, the initial imbalances and spinup have been greatly reduced by introducing an incremental analysis update (IAU) procedure (Bloom et al. 1996).

The NCEP–NCAR reanalysis products were also produced with a fixed assimilation system (Kalnay et al. 1996) consisting of the NCEP Medium Range Forecast spectral model and the operational NCEP spectral statistical interpolation scheme (SSI; Parrish and Derber 1992) with recent improvements. The assimilation was performed at a horizontal resolution of T62 and with 28 sigma levels in the vertical. The implementation of SSI in the analysis makes it unnecessary to employ an initialization step. The NCEP analysis is performed on the model sigma levels employing mandatory pressure-level data and significant-level winds.

The operational ECMWF data assimilation system has undergone a number of changes, which have had a major impact on the character of the data. The impact of changes in the system was especially pronounced during the early and mid 1980s, and particularly so for the divergent wind field and humidity in the Tropics (e.g., Trenberth and Olson 1988; Arpe 1990). The major components of the ECMWF data assimilation system employed for the years of interest here are a multivariate optimal interpolation (OI) scheme, a diabatic nonlinear normal mode initialization scheme (Hollingsworth et al. 1986), and a T106 spectral model with 16 levels, which was changed to 19 levels in May 1986. Changes to the OI scheme during these years are discussed in Trenberth and Olson (1988). The more recent years (since September 1991) employed the ECMWF Integrated Forecast System, which includes a T213 31-level model, an OI scheme, normal mode initialization, and a 1D variational analysis for satellite data (starting in June 1992). The analysis is performed at model levels and significant-level data are used in the analysis.

Although partially constrained by the observational data, the quality of the final assimilation products is strongly influenced by the model physical parameterizations. Those aspects of the model most relevant to the current study include the convection scheme, the planetary boundary layer (PBL) scheme, the land surface scheme, as well as the resolution in the planetary boundary layer (horizontal as well as vertical). In the DAO model, the subgrid penetrative and shallow cumulus convection originating in the boundary layer is parameterized by using the relaxed Arakawa–Schubert (RAS) scheme (Moorthi and Suarez 1992). A simplified Arakawa–Schubert convective parameterization scheme is also utilized in the NCEP model (Pan and Wu 1994). The early versions of the ECMWF model employed a Kuo scheme: this was changed to a mass-flux convection scheme in May 1989 (Tiedtke 1989). The DAO model has the lowest horizontal resolution, whereas the ECMWF model has the highest (see above). In the vertical, the DAO model has four levels below approximately 850 mb and the NCEP model has seven. The ECMWF model has four (five) levels below approximately 850 mb before (after) 1992.

In the DAO model, the turbulent fluxes of momentum, heat, and moisture in the region of the PBL above the surface layer are predicted by the level 2.5 second-order turbulence closure scheme of Helfand and Labraga (1988). This scheme predicts turbulent kinetic energy as a prognostic variable and the remaining second moments as diagnostic variables. The lowest layer of the model corresponds to an atmospheric surface layer for which wind, temperature, and humidity profiles are obtained from Monin–Obukhov similarity theory (see also Helfand and Schubert 1995). For the NCEP model, the surface fluxes are proportional to the difference between values at the surface and in the adjacent atmosphere. The proportionality constants are dependent on wind speed and static stability of the surface layer. Above the surface layer, the turbulent fluxes are expressed as bulk formulas, following Monin–Obukhov similarity theory (Kanamitsu 1989). The PBL height is diagnostically determined from the vertical profile of Richardson number (Troen and Mahrt 1986). In the ECMWF model, the turbulent fluxes of heat, momentum, and moisture are expressed as a function of Richardson number in all layers above the surface layer (Louis 1979); a Monin–Obukhov formulation is used above the PBL height. The surface fluxes are predicted based on a Richardson number formulation (Louis 1979); under neutral conditions the transfer coefficients are determined by a logarithmic profile. The PBL height is diagnostically determined as the height predicted by Ekman theory and the dry convective height associated with Richardson numbers (Louis et al. 1982). In both the NCEP and ECMWF schemes, the turbulent kinetic energy is diagnostically determined. Both the DAO and NCEP models employ a mean orography, while the ECMWF model employed an enhanced envelope orography starting in April 1983.

The soil moisture in the GEOS-1 assimilation system is computed off-line based on a simple bucket model using observed monthly mean surface air temperature and precipitation (Schemm et al. 1992), whereas a simple soil model is included in the NCEP assimilation system (Pan and Mahrt 1987). In the ECMWF model, the soil moisture was predicted in a two-layer model (0.07 m and 0.42 m) prior to 1992 and a four-layer model (0.07 m, 0.21 m, 0.72 m, and 1.89 m) after that (Entekhabi and Eagleson 1989).

In addition to the differences in the assimilation system, there are also differences in the input data, which potentially affects the components of the moisture budget. Significant-level wind data are included in the NCEP and ECMWF analysis systems but not in the DAO system. In the ECMWF analysis, satellite thickness reports (SATEM) are used over the ocean and used only above 100 mb over land. The use of the bogus surface data (POABs) from the Australian Bureau of Meteorology are also assimilated in the NCEP and ECMWF systems.[1] Satellite precipitable water content from TOVS, which are not assimilated in the DAO and NCEP reanalyses, were included in the ECMWF assimilation system in February 1987 and are not used over land after January 1989. In May 1991, the ECMWF analysis system introduced a preselection scheme for NESDIS soundings; a 1D variational technique was introduced to enable cloud-cleared radiance data to be used in the Northern Hemisphere in June 1992.

In addition to the differences in the observations directly assimilated, there are also differences in the boundary conditions employed by the three analysis systems. In the DAO system, the sea surface temperature (SST) is updated using the monthly mean blended SST analyses (Reynolds and Marsico 1993), whereas the NCEP system incorporates the weekly global optimal interpolation SST analyses (Reynolds and Smith 1994). The ECMWF system uses the monthly mean SST data from NCEP with a resolution of $5^\circ \times 5^\circ$, which was changed to $2^\circ \times 2^\circ$ mesh data in November 1989. The major differences between the blended and the optimal interpolation SST analyses are in regions of large SST gradients such as the eastern Pacific (Reynolds and Smith 1994).

The 3D pressure-level data used in this study consist of the four times daily (0000, 0600, 1200, and 1800 UTC) data from the DAO reanalysis, the four times daily data from the NCEP–NCAR reanalysis, and the twice daily (0000 and 1200 UTC) uninitialized ECMWF–TOGA WCRP archives. The DAO output has a horizontal resolution of 2° lat $\times$ 2.5° long at 18 pressure levels (1000, 950, 900, 850, 800, 700, 600, 500, 400, 300, 250, 200, 150, 100, 70, 50, 30, and 20 mb). For the NCEP–NCAR reanalysis, the output was provided at a horizontal resolution of 2.5° lat by 2.5° long at 17 pressure levels (1000, 925, 850, 700, 600, 500, 400, 300, 250, 200, 150, 100, 70, 50, 30, 20 and 10 mb). The ECMWF operational analyses were obtained at a horizontal resolution of 2.5° lat $\times$ 2.5° long at 14 or 15 pressure levels (1000, 925, 850, 700, 500, 400, 300, 250, 200, 150, 100, 70, 50, 30, and 20 mb). The 925-mb level became available beginning in January 1992. Both of the NCEP and ECMWF datasets are further interpolated linearly to the DAO 2° lat $\times$ 2.5° long grid. The vertically integrated moisture flux, $\mathbf{Q}$, is obtained by integrating over the depth of the atmosphere. In σ coordinates, we have

$$\mathbf{Q} = \frac{\pi}{g} \int_0^1 \mathbf{V} q \, d\sigma. \tag{1}$$

Using $dp = \pi \, d\sigma$, we obtain

[1] The bogus data were inadvertently incorporated with a 180° phase shift in the NCEP product.

$$\mathbf{Q} = \frac{1}{g}\int_{p_t}^{p_s} \mathbf{V} q \, dp, \tag{2}$$

where $\mathbf{V}$ is the horizontal wind vector, q the specific humidity, $\pi = p_s - p_t$, g the gravitational acceleration, p_t the pressure at the top of the atmosphere, and p_s the surface pressure. The vertically integrated moisture fluxes from the DAO and NCEP assimilation systems are precomputed in the model σ coordinates. For the DAO product the vertical integrals are accumulated ''on the fly'' at every model time step to eliminate any potential time-sampling problems. For the ECMWF operational analysis, the vertical integration is performed on the available pressure levels. The calculation uses the surface pressure supplied by ECMWF and thus suffers from the problems associated with using an enhanced envelope orography (Trenberth 1995; Trenberth and Guillemot 1995). The impact of the limited vertical resolution of the ECMWF operational analysis is discussed in section 4. The vertically integrated moisture flux convergence is computed employing a fourth-order numerical scheme similar to that used in the GEOS-1 GCM (Suarez and Takacs 1995).

To validate the quality of the precipitation anomalies of the two reanalyses,[2] the NOAA hourly precipitaion data (Higgins et al. 1996) is used for the North America sector, and the observed monthly mean precipitation dataset archived at the Center of Ocean–Land–Atmosphere Studies (COLA) is used for comparison over the Indian monsoon region and the South American sector (courtesy of COLA). The COLA precipitation data were computed by combining the monthly mean gridded station data from the Global Precipitation Climatology Center over land (Janowiak and Arkin 1991) and the precipitation derived from the Microwave Sounding Unit satellite data over ocean (Spencer 1993).

3. Intercomparisons

In this section we compare the vertically integrated regional moisture flux and flux convergence anomalies from the three analyses in the three key regions (see Fig. 1). Regions I and II are the same as those examined by Wang and Paegle (1996), although the current study examines different time periods and has a different emphasis; the focus here is on the ability of the assimilations to capture climate anomalies. Our basic measure of the climate ''signal'' for the ith year monthly mean quantity ($\overline{x}_i$) for each dataset is defined as

$$\frac{\overline{x}_i - [\overline{x}_i]}{[(\overline{x}_i - [\overline{x}_i])^2]^{1/2}} \equiv \frac{\overline{x}_i^*}{\sigma_x}, \tag{3}$$

where bar denotes a monthly mean, the subscript (i) denotes a particular year of a month (say July), and the square brackets denote an average over the nine years (1985–93) for that month. The asterisk (*) denotes the deviation from the 9-yr mean, and the σ_x is the standard deviation in the monthly means. In the following sections we shall show both normalized and unnormalized anomalies.

We begin by examining selected spring and summer months characterized by extreme (drought or flooding) conditions for each region. This is followed by a summary of the overall correspondence in the interannual variability between the three analyses for all months.

a. Climate extremes

1) THE UNITED STATES GREAT PLAINS (REGION I)

The average moisture flow over the Great Plains during the warm season is dominated by an intense low-level southerly flux from the Gulf of Mexico (e.g., Benton and Estoque 1954; Rasmusson 1967; Peixoto and Oort 1983). Interannual variations in this strong southerly wind have been linked to extreme climate anomalies such as droughts and heat waves over the United States (e.g., Namias 1982; Lyon and Dole 1995). Both reanalysis products produce quite realistic precipitation anomalies over the United States compared with station observations during July 1993 and June 1988 (Fig. 2). The major differences are a tendency for both reanalysis products to underestimate the positive precipitation anomaly over the central United States during the flooding conditions and overestimate the negative precipitation anomaly during the drought. In the following we examine the level of agreement in the three analyses in the characterization of the moisture flux and moisture convergence anomalies during July 1993 and June 1988.

Figure 3 shows the spatial distribution of the unnormalized anomalous moisture flux vectors. The light, intermediate, and dark shading indicates regions where the magnitude of the normalized anomalous moisture fluxes [see Eq. (3)] exceeds 1.5, 2, and 2.5 standard deviations, respectively. All three analyses show the basic signature of the wet and dry periods, with much enhanced north/northeastward transport over the central United States during July of 1993, and anomalous southward transport (with magnitude greater than two standard deviations) over much of the eastern half of the United States during the drought. The basic anticyclonic structure of the anomalies during June of 1988 reflects the abnormally strong upper-level anticyclone, which covers much of the country during the drought. Also, anomalous northerly fluxes occur along both coasts during July 1993.

Figure 4 displays the total monthly averaged anomalous moisture flux ($\mathbf{Q}$) for the three analyses integrated along each lateral boundary (see Fig. 1). The moisture fluxes are area weighted and the units are scaled to mm day^{-1}. The inflow and outflow through the boundaries

[2] The precipitation data were not available from ECMWF operational analysis.

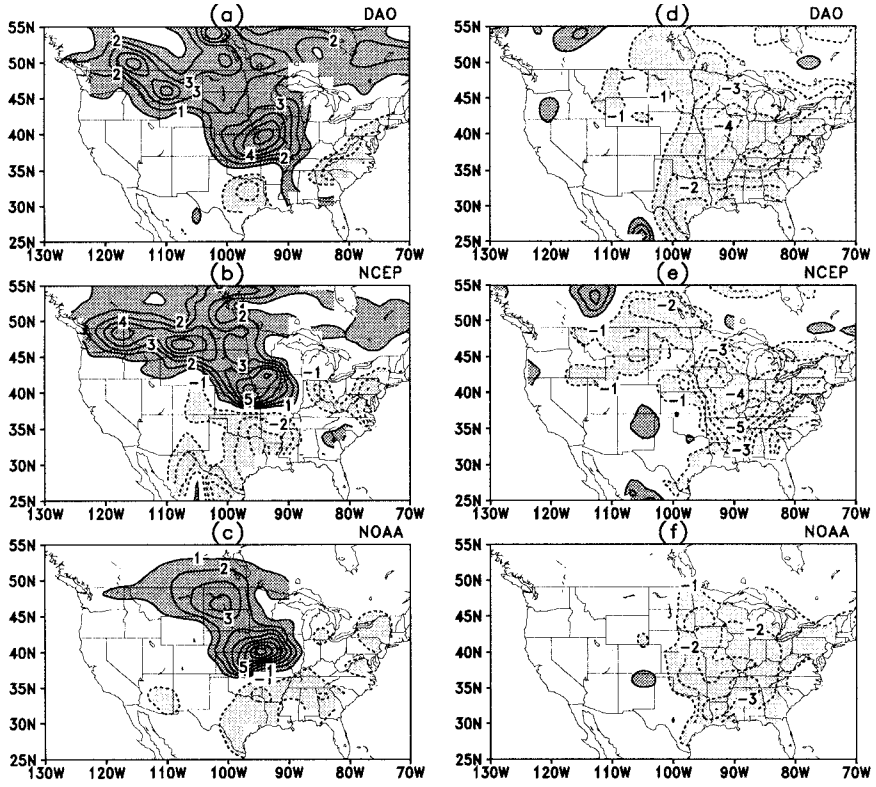

FIG. 2. Precipitation anomalies over the United States for July 1993 (left panel) and June 1988 (right panel) for DAO (top), NCEP (middle), and NOAA station observations (bottom). Contour interval is 1 mm day^{-1}. Dark (light) shadings denote positive (negative) anomalies, respectively. Note that the NOAA station observation dataset is gridded from gauge observations over the continental United States. Thus, values over Canada and Mexico in (c) and (f) are not reliable.

are generally consistent between the three analyses and reflect the anomalies shown in Fig. 3. During the midwest flood conditions in July 1993 (Fig. 4a), all three analyses show anomalous inflow from the southern and western boundaries, and outflow across the eastern and northern boundaries. In comparison to July 1993, the anomalies during June 1988 are reversed (Fig. 4b). In fact, during June 1988 the magnitude of the anomalous outflow from the southern boundary is about twice the magnitude of the anomalous inflow in July 1993.

There are, however, substantial differences between the analyses. For example, the anomalous inflow from the western boundary during July 1993 varies between 1.77 (DAO) and 1.24 (ECMWF), while the anomalous outflow through the eastern boundary varies between 0.84 (DAO) and 0.37 (ECMWF). Surprisingly, the flux convergences differ by much less indicating a tendency for the flux differences across the boundaries to cancel. Substantial differences in the moisture flux anomalies exist as well for June 1988. In particular, the NCEP inflow and outflow along the eastern and western boundaries are substantially weaker than those in the other two analyses.

2) ARGENTINA EAST OF THE ANDES (REGION II)

During summer this region is characterized by a generally northerly low-level flow associated with the result of the extension of the Atlantic anticyclone over the continent and a LLJ along the eastern slope of the Andes. The South American or Pampas LLJ (Paegle 1984) is less well documented than the Great Plains LLJ. This is largely due to the limited observational coverage over this region. There are, for example, few radiosonde observations with generally only one observation per day (1200 UTC). Thus, larger differences (compared with the United States region) are expected in the moisture fluxes, which reflect differences in the assimilation systems. Figure 5 shows the precipitation anomalies for February 1992 and December 1985 over Argentina east of the Andes. During December of 1985 southeastern Brazil experienced drought conditions, while during February 1992 southern Brazil, northern Argentina, and northern Uruguay experienced heavy rains. Compared with observations, both reanalyses produce realistic precipitation anomalies over the South American continent. The major differences between the reanalysis products and the observations occur over the ocean and the moun-

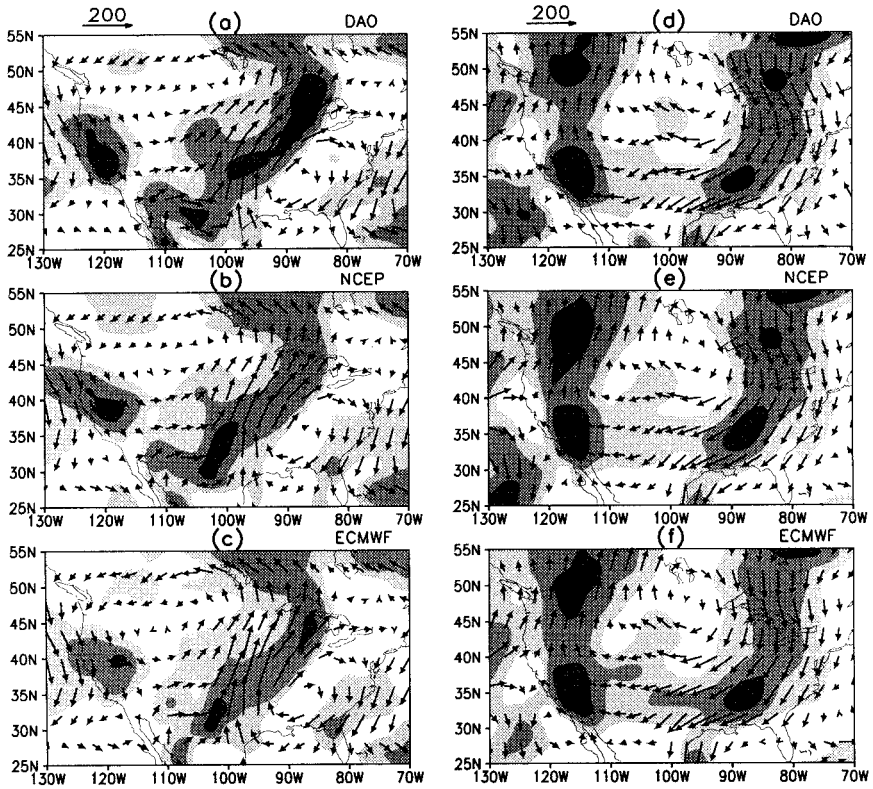

FIG. 3. Anomalies of the vertically integrated moisture fluxes (vectors) and the amplitude of the normalized vertically integrated moisture flux anomalies (shadings) over the United States for July 1993 (left panel) and June 1988 (right panel) for DAO (top), NCEP (middle), and ECMWF (bottom). The unit for vectors is g kg^{-1} m s^{-1} and the scale of vectors is given at the top of the plot. Light, intermediate, and dark shadings denote 1.5, 2, and 2.5 standard deviations, respectively.

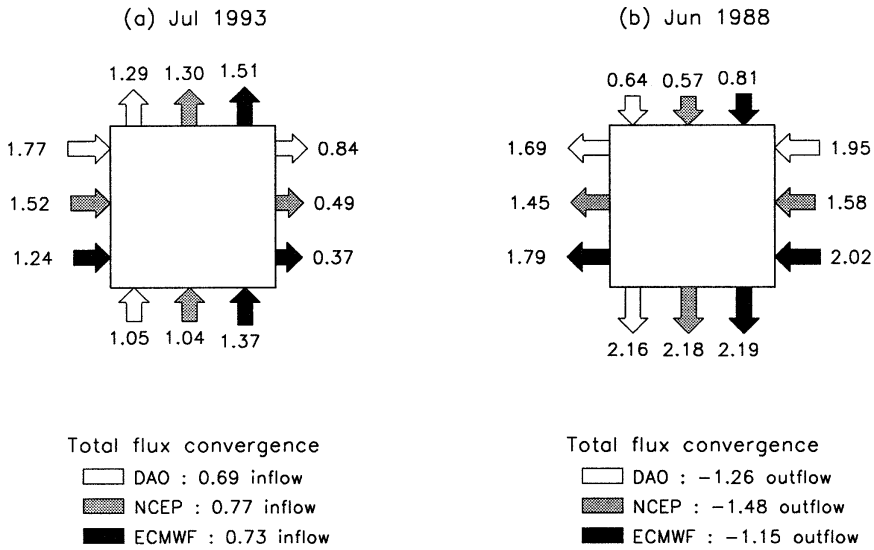

FIG. 4. Anomalies of the vertically integrated moisture fluxes across the lateral boundaries and the area averaged vertically integrated moisture flux convergence over the Great Plains for (a) July 1993 and (b) June 1988 for DAO (blank arrows), NCEP (light-shaded arrows), and ECMWF (heavy-shaded arrows). Units are mm day^{-1}.

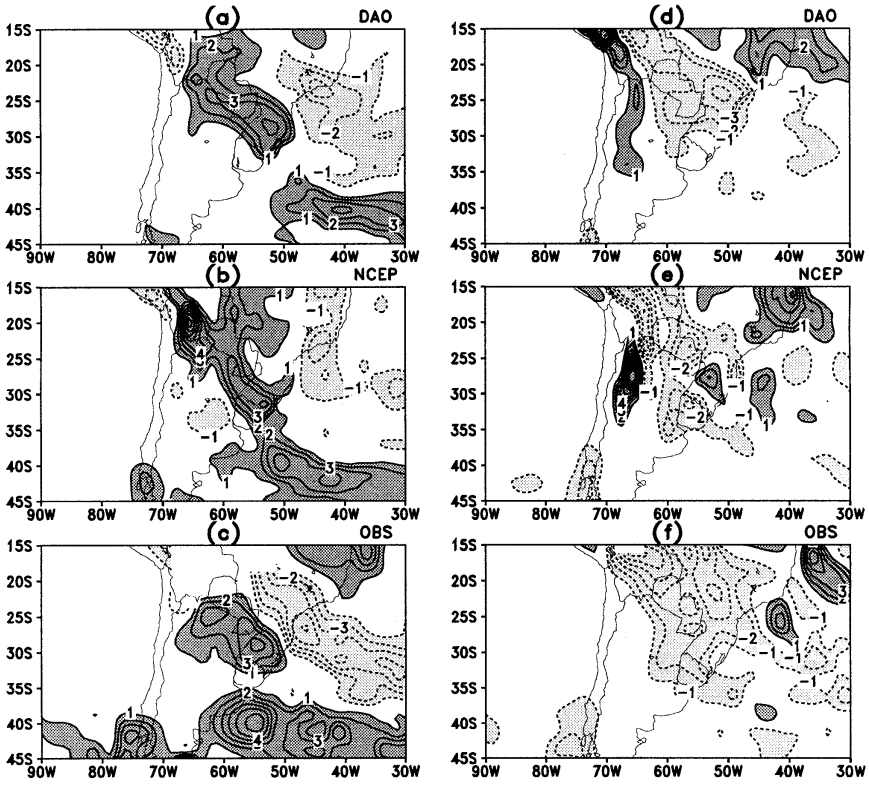

FIG. 5. Precipitation anomalies over South America for February 1992 (left panel) and December 1985 (right panel) for DAO (top), NCEP (middle), and observations (bottom). Contour interval is 1 mm day^{-1}. Dark (light) shading denotes positive (negative) anomalies, respectively.

tain ranges of the Andes. Also, the NCEP–NCAR precipitation field over land tends to be somewhat noisier than either the observations or the DAO product especially for December 1985.

The vertically integrated moisture flux anomalies over South America and adjacent oceans for February 1992 and December 1985 are shown in Fig. 6. During February 1992, all three show an enhanced southward flux east of the Andes and an enhanced anticyclonic flux off the east coast (Fig. 6a). These anomalies are large compared to the average interannual variability with substantial regions of flux exceeding two standard deviations in magnitude. The ECMWF operational product shows the most intense flux anomalies east of the Andes, whereas the NCEP product has the weakest. Both the ECMWF operational and NCEP reanalysis products show the East Coast anticyclonic anomalies extending well inland, whereas this is not the case for the DAO product. During December 1985 (Fig. 6b), the anomalies are southerly and southeasterly over much of the continent. The DAO product shows the largest anomalies north of about 25°S, while both NCEP reanalysis and ECMWF operational analysis have relatively large southerly fluxes extending further south over the continent to about 35°S.

The anomalous moisture fluxes across the lateral boundaries show substantial differences between analyses (Fig. 7). During February of 1992 the influx from the north is almost a factor of 2 smaller in the ECMWF operational product. The inflow from the west ranges between 0.62 mm day^{-1} for the DAO product and 0.25 mm day^{-1} for the ECMWF operational product. The eastern boundary has the largest discrepancy with the ECMWF operational product showing an inflow of more than 2 mm day^{-1} while the DAO product shows essentially no net flux: this reflects the differences in the westward extension of the East Coast anticyclonic anomalies discussed above and the relatively weaker easterly anomalies in the north branch of the anticyclonic anomalies. These differences translate to a large difference in the convergence with the ECMWF operational product showing the largest convergence (0.84 mm day^{-1}) and the DAO product showing a weak divergence. Surprisingly, the December 1985 anomalies are in somewhat better agreement. The exception to this is the eastern boundary, where the ECMWF operational product shows no net flux while both reanalyses show more than 1 mm day^{-1} inflow. In general, the discrepancies are largest at the eastern and western boundaries, reflecting data voids over the ocean and difficulties in the representation of the low-level fluxes over steep topography.

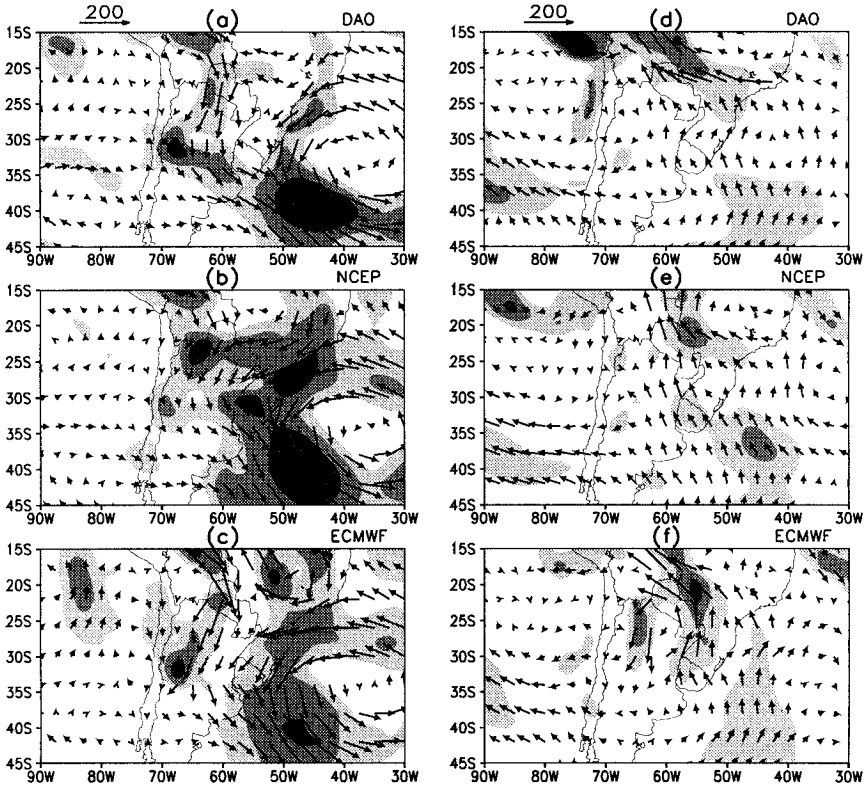

FIG. 6. Same as Fig. 3 except for South America for (a) February 1992 (left panels) and (b) December 1985 (right panel).

3) THE INDIAN MONSOON REGION (REGION III)

The Indian monsoon region was chosen to encompass both the Somali jet and India. The Somali jet is characterized by strong low-level southerly flow near the Somali coastline, which contributes substantially to the cross-equatorial moisture transport and evaporative moisture sources that fuel the Indian monsoon (Murakami et al. 1984). During the summer of 1987 the Indian monsoon was weaker than normal while a much enhanced monsoon occurred during the summer of 1988. The month of May was chosen to highlight the interannual differences in the Somali jet and the onset phase of the monsoon. The reanalyses produce qualitatively similar precipitation anomaly patterns compared to the observations (Fig. 8), with May of 1988 characterized by reduced tropical precipitation off the east coast of Africa, and enhanced precipitation in a region extending from the Arabian Sea, south of India into the Bay of Bengal. During May of 1987 both reanalyses and observation show reduced precipitation over much of the latter region. However, the DAO assimilation extends the Bay of Bengal negative precipitation anomaly too far west over the Indian subcontinent. While there are considerable differences between the reanalyses and the observations, the NCEP–NCAR reanalysis appears to do a better job in depicting the major precipitation anomalies over this region.

The three estimates of the moisture flux anomalies (Fig. 9) again capture similar features. The strong monsoon (May 1988) is characterized by much enhanced westerly flux throughout the Tropics, while the weak monsoon is characterized by substantial easterly flux anomalies south of 10°N. The westerly anomalies during 1988 are quite large (more than two standard deviations) over much of the Tropics in all three products, and the easterly anomalies in 1987 are particularly large just south of India. During May 1987, all three analyses show large (more than two standard deviations) southeasterly anomalies over the Indian peninsula. The spatial patterns of the flux anomalies show substantial differences. During 1988 the westerly anomalies have a clear wavelike structure in the DAO product with a substantial southerly flux component along the east coast of Africa and northerly component near 65°E. In contrast, the ECMWF operational and NCEP reanalysis products show a more zonal structure. The reverse is true for 1987 where the DAO product shows a more zonal structure in the easterly anomalies.

The differences in the moisture flux through the lateral boundaries (Fig. 10) reflect the differences in the flux patterns described above. During May 1988 the DAO product shows a substantially larger outflow through the eastern boundary, and substantially larger inflow at the southern boundary compared with the other

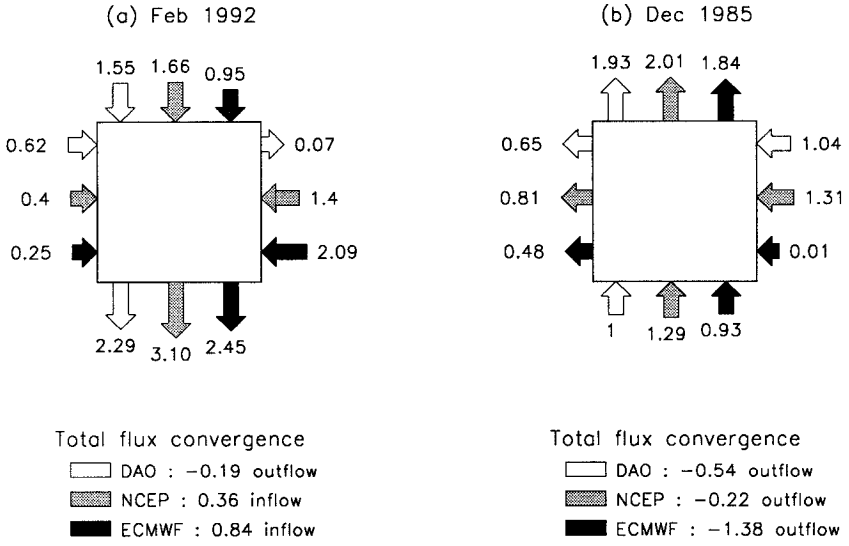

FIG. 7. Same as Fig. 4 except for Argentina east of the Andes for (a) February 1992 and (b) December 1985.

two. The western and northern boundaries show relatively weak fluxes. There is somewhat better agreement during May 1987, but the boundary fluxes tend to be largest in the DAO product. Both years show a net divergence that is strongest in the ECMWF product and weakest in the NCEP product.

A preliminary analysis of the variability over the monsoon region in the DAO product shows a strong dependence of the precipitation anomalies on the availability of the Indian station data (Park et al. 1996). While the operational centers routinely throw out moisture and height observations from certain ''black-listed sta-

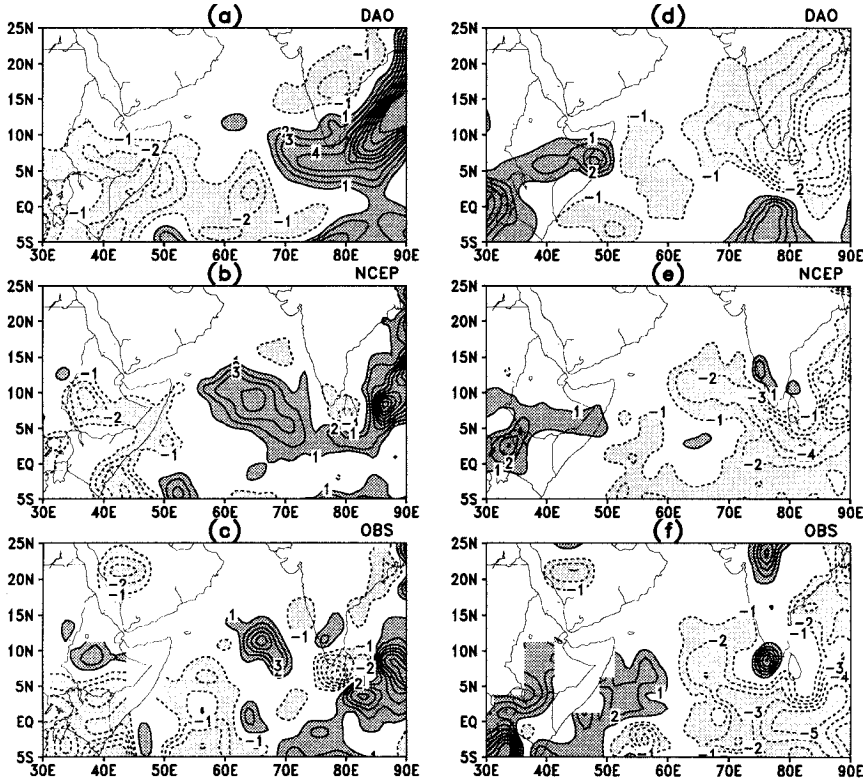

FIG. 8. Same as Fig. 5 except for the Indian monsoon region.

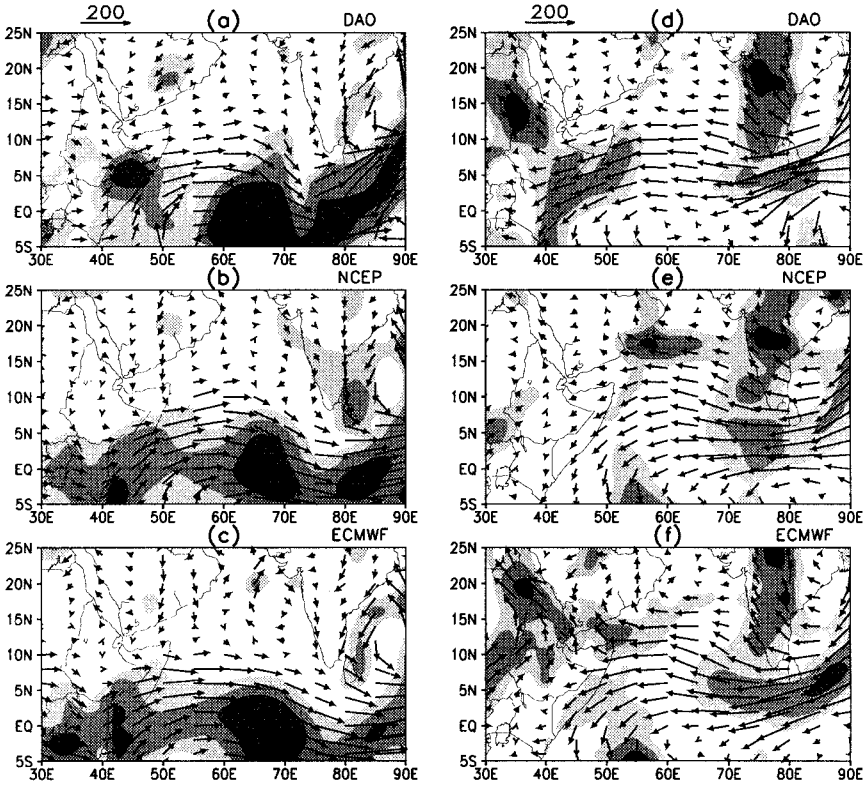

FIG. 9. Same as Fig. 3 except for the Indian monsoon region for May 1988 (left panels) and May 1987 (right panels).

tions,'' this was not the case for the DAO reanalysis. The black-listed observations are primarily over the Indian monsoon region, and to the extent that they passed the internal quality checks are likely responsible for some of the differences in the DAO product in this region.

b. Interannual variability

In this section we examine the degree of correspondence in the spatial patterns of the anomalies in the moisture flux and convergence for all months. The comparison is done in terms of the 9-yr (1985–93) average

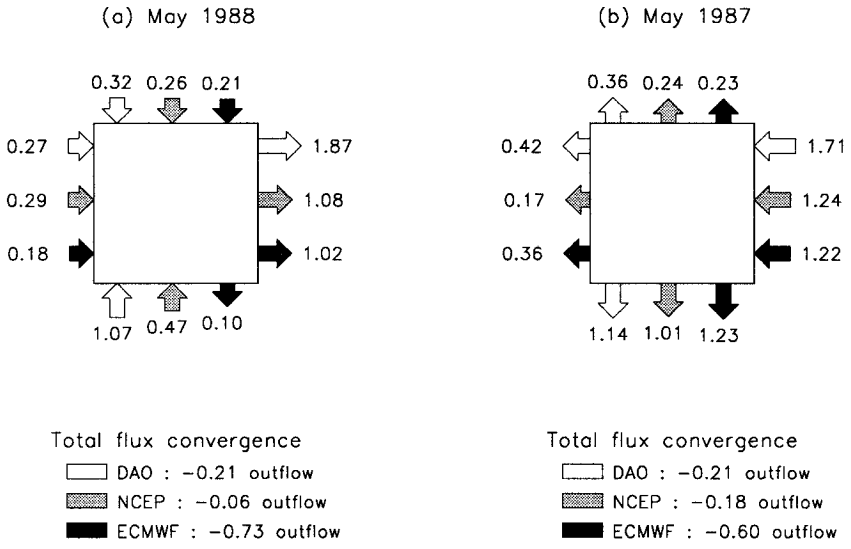

FIG. 10. Same as Fig. 4 except for the Indian monsoon region for (a) May 1988 and (b) May 1987.

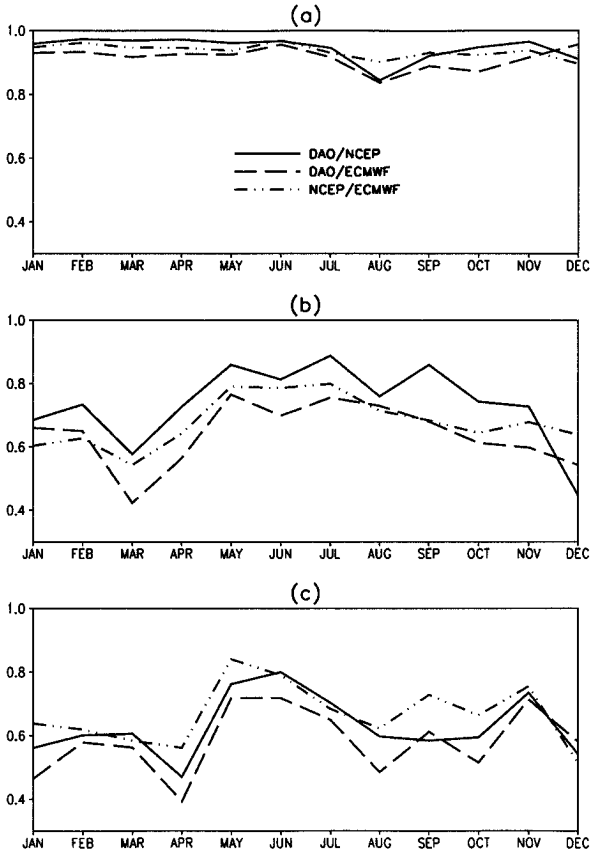

FIG. 11. Seasonal variations of the spatial correlations of the amplitude of the vertically integrated moisture fluxes during the period of 1985–93 for (a) the Great Plains (region I), (b) Argentina east of the Andes (region II), and (c) the Indian monsoon region (region III). The solid lines denote correlations between DAO and NCEP, the dashed lines between DAO and ECMWF, and the dash–dotted lines between NCEP and ECMWF.

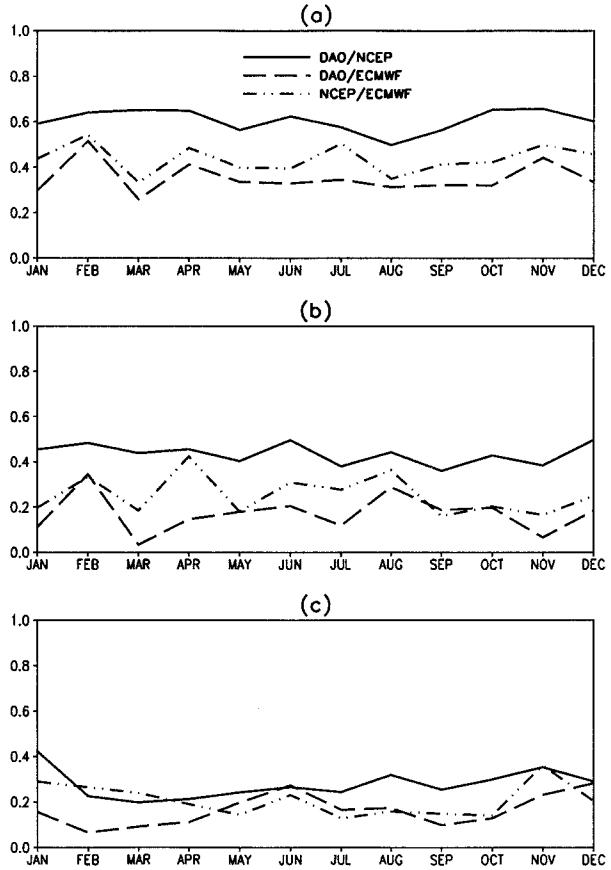

FIG. 12. Same as Fig. 11 except for the vertically integrated moisture flux convergence.

of the spatial correlations of the monthly mean anomalies over the three regions shown in Fig. 1.

Figure 11 shows the spatial correlations for the vertically integrated flux magnitudes in the three regions. The correlations are quite high over the Great Plains (greater than 0.9) throughout the year. There is little evidence of a seasonality in the correlations except for a slight decrease in August involving the correlations with the DAO product. The correlations over the South American region are considerably lower and show a clear seasonal cycle; they are low during summer (about 0.6) and high during winter (about 0.8). The correlations are still lower over the Indian monsoon region, with the correlations reaching 0.8 during only the active monsoon months of late spring and early summer. These results clearly show the impact of the differences in observational coverage in the three regions. This measure does not, however, show a substantial difference in correspondence between the operational and reanalysis products, though there is a slight tendency for the reanalysis products to agree more closely over the Great Plains and the South American regions.

Figure 12 is the same as Fig. 11 except for the vertically integrated flux convergence. The correlations are considerably lower than for the moisture fluxes. This is not surprising, since the convergence is a more sensitive measure (involving derivatives of the fluxes) of the differences between the analyses. The correlations are highest between the reanalysis products averaging about 0.61 for the Great Plains region, 0.44 for the South American region, and 0.28 for the monsoon region. There is surprisingly little seasonality to the correlations, though there is a slight tendency for the NCEP–DAO correlations to be higher during the spring and fall months over the Great Plains. These results suggest that the ability of the assimilated products to capture climate signals in the hydrological cycle, in particular the components of the moisture budget, is rather limited. While the use of unvarying assimilation systems (the reanalyses) appears to result in some improvement (as measured by the correlations), the degree of correspondence is still rather low over data-rich regions, and basically void of information content over data-sparse areas such as over the Indian monsoon region.

We examine next the differences between the three

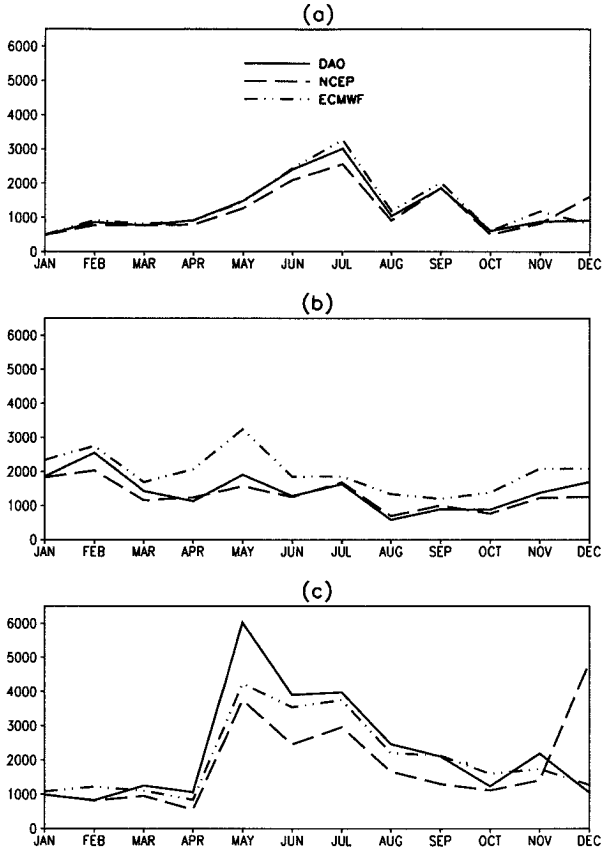

FIG. 13. Seasonal variations of the interannual variances of the amplitude of the vertically integrated moisture fluxes during the period of 1985–93 averaged over (a) the Great Plains (region I), (b) Argentina east of the Andes (region II), and (c) the Indian monsoon region (region III). The solid lines represent the DAO reanalysis, the dashed lines the NCEP reanalysis, and the dash–dotted lines lines the ECMWF operational analysis. Units are $(g\ kg^{-1}\ m\ s^{-1})^2$.

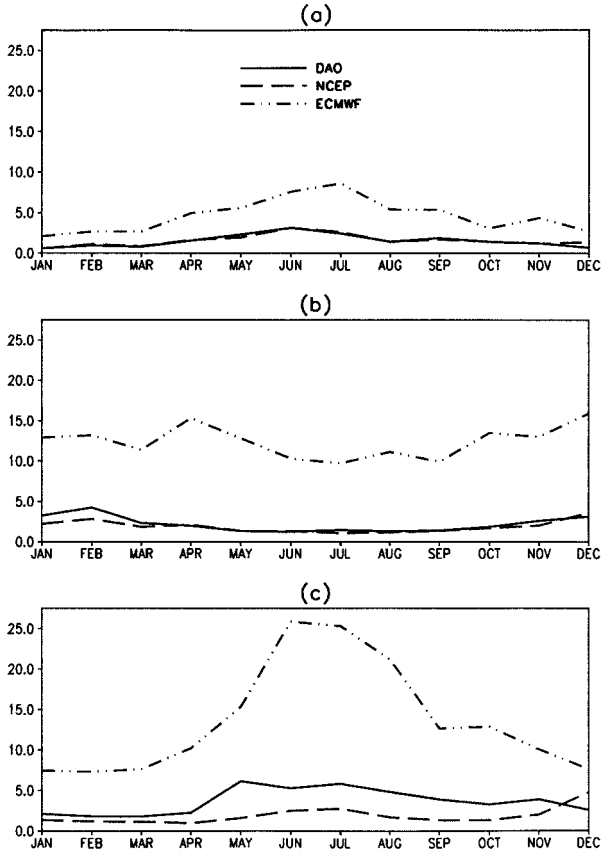

FIG. 14. Same as Fig. 13 except for the vertically integrated moisture flux convergence. Units are $(mm\ day^{-1})^2$.

products in the interannual variance. Figure 13 compares the area-averaged interannual variance of the magnitude of the monthly mean fluxes. In general all three products show similar variances. The ECMWF operational product shows somewhat larger variances than the reanalysis products over the South American region. The poorest agreement is again over the Indian monsoon region. Over the Great Plains region, the largest variance occurs during June and July. The Indian monsoon region shows enhanced variability during May–July, with the largest interannual variability tied to the onset period of summer monsoon (May). Figure 14 compares the variances in the vertically integrated flux convergence. Here the differences between the operational and reanalysis products are evident. In all three regions the ECMWF operational product has substantially more interannual variance (roughly a factor of 3) in the convergence. This reflects the locally more intense convergence patterns in the ECMWF operational product, which may be associated with the spatial resolution of the assimilation system.

4. Uncertainties

In the previous section we have shown that, while there are substantial similarities between the three analyses, there are also major differences that are particularly pronounced in the moisture convergence. In this section we attempt to determine those components of the moisture fluxes and flux convergence that are most responsible for the differences between the three analyses. We begin by comparing the contributions to the interannual variability of the monthly mean moisture fluxes. This is followed by a closer look at the terms contributing to the anomalous flux convergence during the extreme (drought and flood) months examined in the previous section.

a. Moisture flux

The interannual variations in the monthly mean moisture flux result from variations in the monthly means, variations in the monthly mean covariances, and from interannual covariances between the monthly means and monthly mean covariances. This may be written for the northward flux as

$$\mathrm{Var}(vq) = [(\overline{vq} - [\overline{vq}])^2]$$
$$= [(\overline{v}\,\overline{q} - [\overline{v}\,\overline{q}])^2] + \left[\left(\overline{v'q'} - \left[\overline{v'q'}\right]\right)^2\right]$$
$$+ 2\,\mathrm{Cov}\left(\overline{v}\,\overline{q},\ \overline{v'q'}\right), \quad (4)$$

where the bar denotes a monthly average and the square brackets denote a 9-yr mean. The prime indicates a deviation from the monthly mean. The first term on the right-hand side of Eq. (4) may be further decomposed into a term involving the monthly mean variations in the wind, and covariance of monthly mean moisture and wind fields, and other terms as

$$[(\overline{v}\,\overline{q} - [\overline{v}\,\overline{q}])^2] = [\overline{v}^{*2}][\overline{q}]^2 + [\overline{v}][\overline{q}][\overline{v}^*\overline{q}^*]$$
$$+ \text{ other terms}, \quad (5)$$

where the other terms include, for example, $[\overline{q}^{*2}][\overline{v}]^2$, which is the contribution due to the monthly mean moisture variations. Note that the asterisk (*) indicates a deviation from the 9-yr mean. In the following we show profiles of the various contributions to the variance in the meridional flux at several locations. The locations and months are chosen to highlight the differences in the variability of the LLJs in each of the three regions shown in Fig. 1.

Figure 15 shows components of the meridional flux variance profile for July over the Great Plains in a region where the LLJ is active (30°–40°N, 95°–105°W). The interannual variance in the monthly mean flux is dominated by the term involving the variance in the monthly mean winds [first term on the right-hand side of Eq. (5) shown in Fig. 15a]. The DAO product shows a more intense low-level variance maximum than the other products with the maximum occurring at 950 mb, while in the ECMWF operational and NCEP reanalysis products the maximum occurs at 850 mb and 925 mb, respectively. The pressure-level data of the ECMWF operational analysis clearly has insufficient resolution to resolve the low-level maximum. The differences in the level of the maximum between NCEP and DAO (950 vs 925 mb) very likely reflect the differences in output levels; however, the differences in magnitude appear to be real. The ECMWF operational product shows more variance than the other products above 850 mb. The remaining terms (Fig. 15b) are approximately an order of magnitude smaller in which the contribution due to the covariance of the monthly mean moisture and wind fields is the most significant [second term in Eq. (5)]. Figures 15c and 15d show the wind variance and mean-square moisture profiles, respectively, making up the dominant term in the flux variance [first term on rhs of Eq. (5)]. The differences in the variance of the moisture flux clearly reflect the differences in the variances of the boundary layer winds, though the wetter ECMWF moisture profile contributes substantially to the differences at 850 mb and above. Table 1 quantifies the relative contributions to the flux discrepancies at 850 mb, which is the lowest level at which all three centers provide data. This shows a distinct difference between the reanalysis and operational products for the Great Plains such that wind discrepancies dominate the reanalysis differences, while both wind and moisture discrepancies are important for the differences with the operational product.

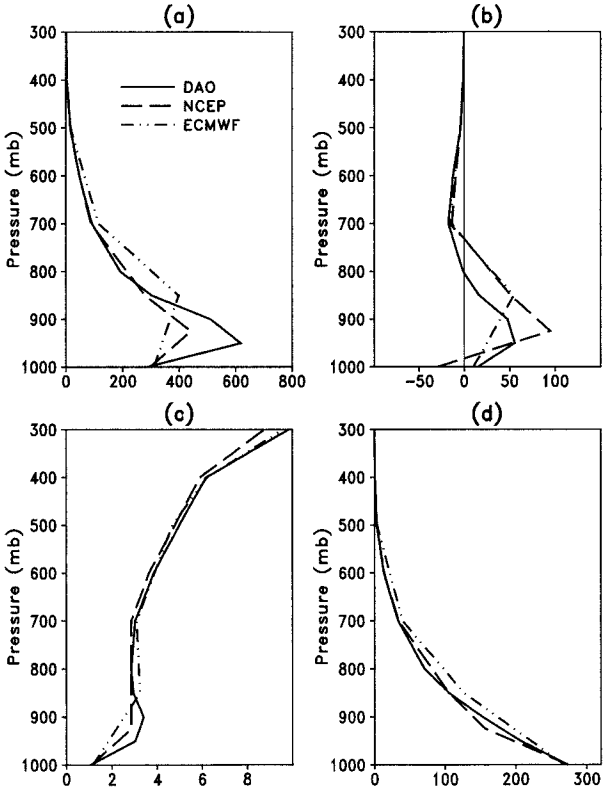

FIG. 15. The vertical profiles of the contributions to the interannual variances of the meridional moisture flux averaged over 30°–40°N and 95°–105°W for July from (a) the interannual variances in the monthly mean meridional wind weighted by the square of the 9-yr averaged monthly mean moisture profiles [first term in Eq. (5)] and (b) the remaining terms in Eq. (4) and (5). Panels (c) and (d) show the vertical profiles of the interannual variances of the monthly mean meridional wind and the square of the 9-yr averaged monthly mean moisture profiles, respectively, which makes up the variance profiles in (a). The solid lines represent the DAO reanalysis, the dashed lines the NCEP reanalysis, and the dash–dotted lines the ECMWF operational analysis. The units are $(\mathrm{g\ kg^{-1}\ m\ s^{-1}})^2$ for (a) and (b), $(\mathrm{m\ s^{-1}})^2$ for (c), and $(\mathrm{g\ kg^{-1}})^2$ for (d).

Figure 16 shows the components of the February meridional flux variance over South America just east of the Andes Mountains (20°–30°S, 55°–65°W). The dominant term [first term on rhs of Eq. (5) in Fig. 16a] is considerably different among the three analyses. The DAO and NCEP estimates have the maximum below 850 mb (950 and 925 mb, respectively), though the DAO maximum is about three times that of NCEP. The ECMWF operational product again does not have sufficient resolution to distinguish this maximum, but the variance at 850 mb is about twice that of the DAO product and four times that of the NCEP product. The

TABLE 1. The differences (Δ) between two analyses of the quantity $[\bar{v}^{*2}][\bar{q}]^2$ at 850 mb divided by the average of the two corresponding analyses ($\sim$) of the individual components

$$\left\{\frac{\Delta([\bar{v}^{*2}][\bar{q}]^2)}{\widetilde{[\bar{v}^{*2}][\bar{q}]^2}} = \frac{\Delta([\bar{v}^{*2}])}{\widetilde{[\bar{v}^{*2}]}} + \frac{\Delta([\bar{q}]^2}{\widetilde{[\bar{q}]^2}}\right\}.$$

The ratios are area averaged.

	Great Plains		
	NCEP − DAO	ECMWF − DAO	ECMWF − NCEP
$\frac{\Delta([\bar{v}^{*2}])}{\widetilde{[\bar{v}^{*2}]}}$	−0.034	0.094	0.128
$\frac{\Delta([\bar{q}]^2)}{\widetilde{[\bar{q}]^2}}$	0.000	0.183	0.183
$\frac{\Delta([\bar{v}^{*2}][\bar{q}]^2)}{\widetilde{[\bar{v}^{*2}][\bar{q}]^2}}$	−0.034	0.277	0.311
	Argentina east of the Andes		
	NCEP − DAO	ECMWF − DAO	ECMWF − NCEP
$\frac{\Delta([\bar{v}^{*2}])}{\widetilde{[\bar{v}^{*2}]}}$	−0.601	0.149	0.734
$\frac{\Delta([\bar{q}]^2)}{\widetilde{[\bar{q}]^2}}$	−0.066	0.360	0.423
$\frac{\Delta([\bar{v}^{*2}][\bar{q}]^2)}{\widetilde{[\bar{v}^{*2}][\bar{q}]^2}}$	−0.667	0.509	1.157
	Indian monsoon region		
	NCEP − DAO	ECMWF − DAO	ECMWF − NCEP
$\frac{\Delta([\bar{v}^{*2}])}{\widetilde{[\bar{v}^{*2}]}}$	−0.231	−0.162	0.070
$\frac{\Delta([\bar{q}]^2)}{\widetilde{[\bar{q}]^2}}$	−0.267	0.122	0.386
$\frac{\Delta([\bar{v}^{*2}][\bar{q}]^2)}{\widetilde{[\bar{v}^{*2}][\bar{q}]^2}}$	−0.498	−0.040	0.456

remaining terms (Fig. 16b) are again about an order of magnitude smaller. The decomposition of the dominant term [first term on RHS of Eq. (5)] shows that again the differences in the flux variances are strongly influenced by differences in the winds (Figs. 16c and 16d). The ECMWF operational product has the largest lower tropospheric wind variance with a maximum at 700 mb. The NCEP and DAO wind variance profiles show a rather flat variance profile in the lower troposphere, though the NCEP values are considerably weaker than those of the DAO. Here also, the ECMWF operational product is wetter at 850 mb and above. Table 1 shows the relative contributions to the discrepancies for this region are similar to the Great Plains region such that wind differences dominate for the reanalysis products and both wind and moisture differences are important for explaining the differences with the operational product.

The Indian monsoon region (Fig. 17) shows the least interannual variability in the moisture flux of the three

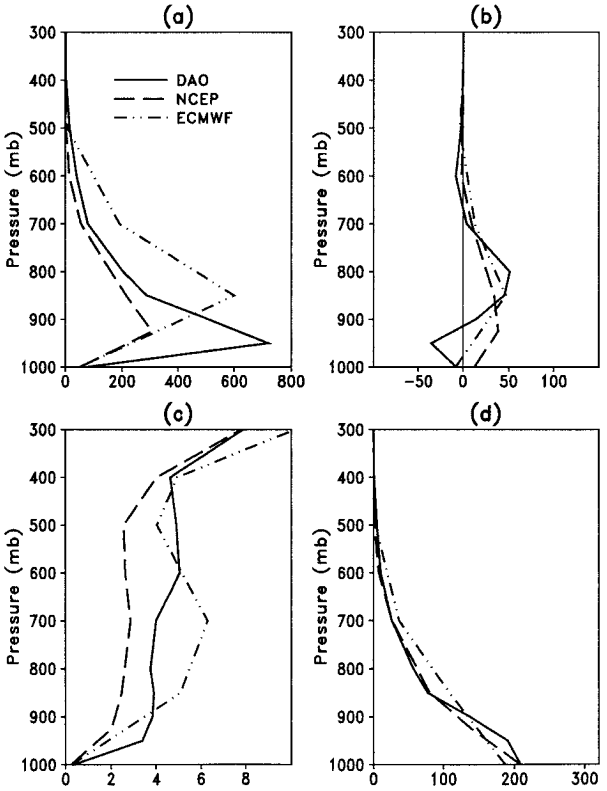

FIG. 16. Same as Fig. 15 except for 20°–30°S and 55°–65°W for February.

regions considered. The meridional flux variance for May in the vicinity of the Somali jet (0°–10°N, 40°–50°E) is only about half that of the other regions. This is due to the smaller variance of the meridional wind (Fig. 17c). The flux variance is again dominated by the wind variance (cf. Figs. 17a and 17b). While the DAO reanalysis and ECMWF operational products show similar flux profiles above 850 mb, this appears to be fortuitous reflecting compensating differences in the wind variances and moisture profiles (cf. Figs. 17c and 17d). The NCEP profile is driest while the ECMWF profile is the wettest. On the other hand, the NCEP reanalysis and ECMWF operational products have similar wind variance profiles (Fig. 17c) while the DAO product shows larger wind variance above 850 mb. In contrast to the other two regions, both the differences in the wind variance and moisture profiles in this region contribute substantially to the differences in the interannual variability of the moisture flux at 850 mb for all three products (Table 1).

b. Moisture convergence

The previous section examined the sources of uncertainty in the estimates of the interannual variability in the monthly mean moisture flux. In this section we examine the uncertainty of the variability of the moisture

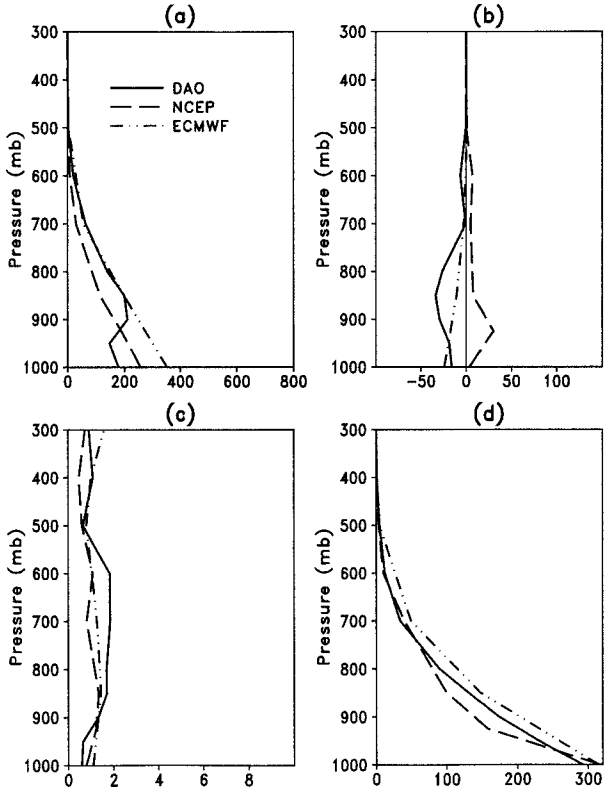

FIG. 17. Same as Fig. 15 except for 0°–10°N and 40°–50°E for May.

convergence. Here we will focus on the drought and flood years during which it is expected that this more sensitive measure of the product quality will be most robust. To help isolate the sources of discrepancy, we decompose the monthly mean moisture flux convergence, $-\overline{\nabla\cdot q\mathbf{V}}$, into its component terms. The monthly averaged moisture flux convergence at a particular level may be written as

$$-\overline{\nabla\cdot q\mathbf{V}} = -\overline{q}\nabla\cdot\overline{\mathbf{V}} - \overline{\mathbf{V}}\cdot\nabla\overline{q} - \nabla\cdot\overline{q'\mathbf{V}'}, \qquad (6)$$

where the first term on the rhs is the contribution from the mean divergent wind field, the second term is the horizontal advection of moisture, and the last term is the contribution from the submonthly transients. The submonthly transient term is computed from the daily mean data so that the diurnal variations are excluded. In the following we compare for each region the area-averaged deviation of each term in Eq. (6) from its corresponding long-term (9-yr) mean.

Here we shall also focus on a particular level to avoid the additional uncertainties imposed by the differences in the available levels of the three products. Table 2 lists the monthly mean deviations from the long-term mean of the individual terms in Eq. (6) at 850 mb averaged over the three key regions. Over the United States Great Plains during July 1993, the contributions from transients and horizontal moisture advection are very consistent in the two reanalysis products. The anomalous convergence is dominated by the mean flow terms with the largest contribution coming from the divergence term. The transients, however, contribute only a small portion to the moisture convergence. The ECMWF operational product, on the other hand, shows the contribution to the convergence anomaly coming almost exclusively from the divergence term.

TABLE 2. Anomalies of $-\nabla\cdot\mathbf{V}q$, $-\overline{q}\nabla\cdot\overline{\mathbf{V}}$, $-\overline{\mathbf{V}}\cdot\nabla\overline{q}$, and $-\nabla\cdot\mathbf{V}'q'$ at 850 mb averaged over the three key regions for selected months. Units: 10^{-5} g kg^{-1} s^{-1}.

	Dataset	$-\nabla\cdot\overline{\mathbf{V}q}$	$-\overline{q}\nabla\cdot\overline{\mathbf{V}}$	$-\overline{\mathbf{V}}\cdot\nabla\overline{q}$	$-\nabla\cdot\mathbf{V}'q'$
	Great Plains				
July 1993	DAO	0.58	0.51	0.14	−0.06
	NCEP	0.54	0.34	0.21	−0.01
	ECMWF	0.40	0.36	−0.01	0.05
June 1988	DAO	−0.30	−0.23	0.11	−0.18
	NCEP	−0.64	−0.38	−0.02	−0.24
	ECMWF	−0.40	−0.42	0.11	−0.09
	Argentina east of the Andes				
February 1992	DAO	0.25	0.35	0.06	−0.16
	NCEP	0.47	0.40	0.18	−0.11
	ECMWF	0.26	0.18	0.17	−0.09
December 1985	DAO	−0.46	−0.42	−0.18	0.14
	NCEP	−0.69	−0.51	−0.30	0.12
	ECMWF	−0.43	−0.12	−0.28	−0.03
	Indian monsoon region				
May 1988	DAO	−0.11	−0.07	−0.16	0.12
	NCEP	−0.05	0.12	−0.17	0.00
	ECMWF	−0.39	−0.16	−0.24	0.01
May 1987	DAO	0.03	−0.19	0.18	−0.02
	NCEP	0.01	−0.18	0.18	0.02
	ECMWF	−0.17	−0.46	0.28	0.01

During June 1988 there is somewhat more disagreement among the three products; however, all three products show that the submonthly transients play an important role in contributing to the anomalous divergence during that time (though less so for the ECMWF operational product). Note that the importance of the submonthly transients to the total divergence anomaly contrasts with the previous section, which showed that the interannual flux variability associated with the intramonthly wind and moisture variations is relatively small. This highlights the important dynamical consequences of small differences in the submonthly wind and moisture covariances, which can generate divergences/convergences of magnitudes comparable to those associated with the monthly mean flows.

The South American region shows qualitatively the same result in all three products with anomalous convergence during February 1992 and anomalous divergence during December 1985. The NCEP product, however, shows substantially larger magnitudes. This is primarily the result of a stronger divergence term in the NCEP product. In both months, the mean flow contribution dominates the anomalous convergence/divergence. The contribution from the transients is similar during February 1992 (all products show divergence),

while during December 1985 the reanalysis products show convergence and the ECMWF operational product shows a slight divergence.

The Indian monsoon region shows little net anomalous convergence in the two reanalysis products during the two months (May 1987 and May 1988). In contrast, the operational product shows a substantial divergence anomaly during both months. These discrepancies are largely the result of differences in the divergence term. The transients contribute little to the total anomalous flux convergence/divergence in this region during both months.

5. Summary and conclusions

The accurate representation of the hydrological cycle is one of the most challenging problems facing the data assimilation community since the quality of the final assimilated products depends strongly on the quality of the observations, the ability of the system to ingest the observations without shocking the hydrological component, and the veracity of the physical parameterizations. The moisture field, characterized by sharp gradients and largely confined to the planetary boundary layer, is inadequately sampled by conventional observations. Current satellite measurements provide substantially improved horizontal coverage, but little information about the vertical distribution. The important role of highly confined low-level jets with strong diurnal cycles makes it clear that current wind observations are inadequate to accurately estimate moisture fluxes and convergence (see, e.g., Rasmusson 1968; Helfand and Schubert 1995). Data assimilation, on the other hand, has the potential for providing global, consistent, and more accurate (than observations alone) estimates of all components of the hydrological cycle. That this potential is not yet fully realized reflects to a large extent the sensitivity of the assimilated hydrological cycle to some of the most difficult aspects of model formulation involving precipitation, clouds, and evaporation, as well as uncertainties in the representation of the planetary boundary layer (see, e.g., Paegle and Vukicevic 1987; Trenberth and Olson 1988; Trenberth 1991; Schubert et al. 1995; Wang and Paegle 1996; Higgins et al. 1996).

This study attempts to shed some light on the quality of current estimates of climate (interannual) anomalies in the hydrological cycle by comparing results from recent operational weather and climate data assimilation systems. One of the distinguishing features of this study is that we focus on variability. The working assumption being that while the products still have strong climate bias, they may, nevertheless, provide more reasonable estimates of variability. That this may be the case is suggested by a number of studies employing the GEOS-1 reanalysis (e.g., Schubert et al. 1995; Schubert and Rood 1995). The focus here is on regions with strong low-level jets and on periods with extreme (drought or flood) conditions in order to determine the ability of the systems to capture the signature of these key processes during major climate events. In particular, moisture fluxes and moisture convergence have been investigated for selected months over the United States Great Plains, Argentina east of the Andes Mountains, and the Indian monsoon region. The assimilated data consist of reanalysis products generated at the NASA/Goddard Data Assimilation Office (Schubert et al. 1993) and the National Centers for Environmental Prediction–National Center for Atmospheric Research (Kalnay et al. 1995), and the operational products of the European Centre for Medium-Range Forecasts. The assimilation systems differ in the general circulation models employed, the assimilation techniques, and the input data. We note that ECMWF is also producing a reanalysis product (Gibson et al. 1994), though it was not available to us in time for this project.

In general, all three products capture the anomalous moisture transports during the dry and wet periods over the key regions. The reanalysis products, in particular, show good agreement in depicting the different roles of the mean flow and transients during the flood and drought periods. There are, however, substantial differences (in both direction and magnitude) between the analyses in the moisture flux anomalies even over regions with relatively abundant observations, which result in substantial differences in the vertically integrated and area-averaged flux convergence. These differences range from 25% over the Great Plains to more than 100% over the other regions. The spatial correlations of the anomalies in the flux magnitude (flux convergence) range from about 0.95 (0.61) over the Great Plains to 0.6 (0.15) over the Indian monsoon region. The correlations tend to be higher between the reanalysis products than with the operational product; however, the rather low correlations for the flux convergence suggest that the ability of assimilation systems to capture climate signals in the hydrological cycle is still limited. One of the largest differences between the operational and reanalysis products occurs in the estimates of interannual variance of the local flux convergence. It is shown that the ECMWF operational product has substantially more variance (roughly a factor of 2) in the flux convergence. This reflects the generally noisier and locally more intense convergence patterns of the operational product.

The sources of uncertainty in the moisture flux anomalies were investigated by separating the interannual variance of the monthly mean moisture flux into its component terms. The dominant term involves the monthly wind variance weighted by the square of the mean moisture profile. Typically, other terms are about an order of magnitude smaller (the covariance between the monthly mean wind and moisture is the most important of the remaining terms). Thus differences in estimates of interannual variability of the flux occur primarily as a result of differences in the variability of the winds and/or as a result of bias in the moisture

profiles. Of these two, the differences in the variability of the lower tropospheric winds is by far the dominant source of the discrepancies in the moisture flux for the reanalysis products in middle latitudes. Only in the Indian monsoon region, where interannual variability in the low-level winds is comparatively small, does the moisture bias play a substantial role. The above result is not true for the operational product where differences in moisture are comparable to the differences in the wind in all three regions.

The sources of uncertainty in the area-averaged anomalous flux convergence was determined by examining the relative contributions to the monthly mean convergence from the mean flow and submonthly transients during the extreme (flood and drought) climate events. While discrepancies in the anomalous divergence often dominate the discrepancies in the flux convergence, this was found to be not universally true. In fact, the relative contributions to the flux convergence anomalies varied considerably by year and region. For example, over the Great Plains during July 1993 the magnitude of the mean flow advection term was about half that of the divergence term, yet estimates of the advective term between analyses varied by more than 100% while those for the divergence term varied by only about 40%.

There are also a number of postprocessing issues that may account for some of the differences. This is especially true for the operational analysis. The vertical integration is done on the available mandatory pressure levels for the ECMWF operational product while it is done on the model sigma level for the reanalyses. Comparisons of sigma level versus pressure level fields employing the DAO products (not shown) indicates differences of about 30% in the area-weighted vertically integrated moisture convergence. This result is consistent with the findings of Trenberth (1995). The vertical interpolation for the ECMWF operational product is also impacted by errors in the surface pressure field, which is based on an enhanced envelope orography (see Trenberth 1992). The conversion from the high-resolution ECMWF operational analysis data to the $2.5^\circ \times 2.5^\circ$ fields may have introduced aliasing in the coarse resolution fields as discussed by Trenberth and Solomon (1993). Also, the operational product is available only twice daily while the reanalyses are provided four times daily, which may lead to large differences over regions with large diurnal and semidiurnal variations (Trenberth 1991). Wang and Paegle (1996) demonstrated that the discrepancies in the moisture flux convergence are reduced by using four times daily data. Other differences involve the amount of data (observations) that were actually ingested by the assimilation systems. For example, the DAO (GEOS-1) assimilation system did not analyze 925 mb or significant level observations. The DAO product also appears to be impacted in the monsoon region by observations from black-listed stations that survived the internal quality checks (Park et al. 1996).

The ultimate source of the discrepancies discussed above is clearly tied to a combination of inadequate observations and model deficiencies especially in regions of steep topography and strong highly confined low-level winds. The lack of observations clearly played a role in the discrepancies over the Indian monsoon region, and also over the South American region, both near the Andes and the adjacent oceans where shifts in the position of the oceanic anticyclone played an important role. It is also clear that the proper representation of the low-level jets is critical for obtaining proper estimates of the anomalous flux convergences. Small differences in the structure and position of the winds in regions of high humidity lead to large differences in the convergence. These problems are not unique to estimating these climate anomalies and have been cited as the main sources of discrepancies in the moisture budget in several previous studies (e.g., Wang and Paegle 1996). While it is encouraging that for the cases studied here all three analyses appear to capture the basic flux anomalies, they are not yet accurate enough to produce reliable quantitative estimates of flux convergence anomalies. Future modeling efforts must clearly lie in improved representation of the boundary layer and orography. Better observations of moisture and especially low-level wind fields would clearly help. Some of the new satellite measurements, which will become available in the next few years, such as those from NASA's Earth Observing System (EOS) Program, should help in that regard. The data assimilation community must also focus on finding better ways of incorporating moisture information from existing sensors, as well as, finding new ways to incorporate unconventional quantities such as cloud and precipitation information (e.g., Krishnamurti et al. 1991, 1993, 1994; Kasahara et al. 1994). In the absence of improved global wind measurements we must, however, rely increasingly on our ability to model the planetary boundary layer. The sensitivity of the fluxes and convergence to the representation of LLJs suggests a renewed emphasis must be placed on understanding and modeling these phenomena.

Acknowledgments. We are very grateful to Wayne Higgins for providing the NCEP–NCAR reanalysis data and the NOAA hourly precipitation data and to Rex Gibson and his colleagues for kindly providing us with information on the history of the ECMWF operational analysis system. The monthly mean observed precipitation data are kindly provided by the Center of Ocean–Land–Atmosphere Studies (COLA). Rex Gibson and his colleagues and two anonymous reviewers provided valuable comments that helped improve the manuscript. Thanks also go to Chung-Kyu Park and Yehui Chang for helpful discussions. This work was supported by NASA's Earth Observing Systems (EOS) projects on 4D Data Assimilation and Computing.

REFERENCES

Arpe, K., 1990: Impacts of changes in the ECMWF analysis-forecasting scheme on the systematic error of the model. *Ten Years of Medium-Range Weather Forecasting,* Vol. 1, Shinfield Park, Reading, United Kingdom, European Center for Medium Range Weather Forecasts, 69–114.

Benton, G. S., and M. A. Estoque, 1954: Water-vapor transfer over the North American continent. *J. Meteor.,* **11,** 462–477.

Bloom, S. C., L. L. Takacs, A. M. DaSilva, and D. Ledvina, 1996: Data assimilation using incremental analysis updates. *Mon. Wea. Rev.,* **124,** 1256–1271.

Bonner, W. D., 1968: Climatology of the low level jet. *Mon. Wea. Rev.,* **96,** 833–850.

——, and J. Paegle, 1970: Diurnal variations in the boundary layer winds over the south-central United States in summer. *Mon. Wea. Rev.,* **98,** 735–744.

Entekhabi, D., and P. S. Eagleson, 1989: Land surface hydrology parameterization for atmospheric general circulation models including subgrid scale spatial variability. *J. Climate,* **2,** 816–831.

Gibson, J. K., P. Kallberg, A. Nomura, and S. Uppala, 1994: The ECMWF re-analysis (ERA) project—Plans and current status. Preprints, *10th Int. Conf. on Interactive Information and Processing Systems for Meteorology, Oceanography and Hydrology,* Nashville, TN, American Meteorological Society, 164–167.

Helfand, H. M., and J. C. Labraga, 1988: Design of a nonsingular level-2.5 second-order closure model for the prediction of atmospheric turbulence. *J. Atmos. Sci.,* **45,** 113–132.

——, and S. D. Schubert, 1995: Climatology of the simulated Great Plains low-level jet and its contribution to the continental moisture budget of the United States. *J. Climate,* **8,** 784–806.

Higgins, R. W., K. C. Mo, and S. D. Schubert, 1996: The moisture budget of the central United States in spring as evaluated in the NMC/NCAR and the NASA/DAO reanalyses. *Mon. Wea. Rev.,* **124,** 939–963.

Hollingsworth, A., D. B. Shaw, P. Lönnberg, L. Illari, K. Arpe, and A. J. Simmons, 1986: Monitoring of observation and analysis quality by a data assimilation system. *Mon. Wea. Rev.,* **114,** 861–879.

Janowiak, J. E., and P. A. Arkin, 1991: Rainfall variations in the tropics during 1986–1989, as estimated from observations of cloud-top temperature. *J. Geophys. Res.,* **96,** 3359–3373.

Kalnay, E., and Coauthors, 1995: The NMC/NCAR Reanalysis Project. *Bull. Amer. Meteor. Soc.,* **77,** 437–471.

Kanamitsu, M., 1989: Description of the NMC global data assimilation and forecast system. *Wea. Forecasting,* **4,** 334–342.

Kasahara, A., A. P. Mizzi, and L. J. Donner, 1994: Diabatic initialization for improvement in the tropical analysis of divergence and moisture using satellite radiometric imagery data. *Tellus,* **46A,** 242–264.

Krishnamurti, T. N., J. Xue, H. S. Bedi, K. Ingles, and D. Oosterhof, 1991: Physical initialization for numerical weather prediction over the tropics. *Tellus,* **43AB,** 53–81.

——, H. S. Bedi, and K. Ingles, 1993: Physical initialization using SSM/I rain rates. *Tellus,* **45A,** 247–269.

——, G. Rohaly, and H. S. Bedi, 1994: On the improvement of precipitation forecast skill from physical initialization. *Tellus,* **46A,** 598–614.

LeComte, D., 1986: The return of the rain: The weather of 1985. *Weatherwise,* **39,** 8–15.

——, 1993: Highlights around the world. *Weatherwise,* **46,** 14–17.

Louis, J. F., 1979: A parametric model of vertical eddy fluxes in the atmosphere. *Bound.-Layer Meteor.,* **17,** 187–205.

——, M. Tiedtke, and J. F. Geleyn, 1982: A short history of the PBL parameterization at ECMWF. *Proc. ECMWF Workshop on Planetary Boundary Layer Parameterization,* Reading, United Kingdom, ECMWF, 59–80.

Lyon, B., and R. M. Dole, 1995: A diagnostic comparison of the 1980 and 1988 U.S. summer heat wave-droughts. *J. Climate,* **8,** 1658–1975.

Matsuyama, H., 1992: The water budget in the Amazon river basin during the FGGE period. *J. Meteor. Soc. Japan,* **70,** 1071–1084.

——, T. Oki, M. Shinoda, and K. Masuda, 1994: The seasonal change of the Congo River Basin. *J. Meteor. Soc. Japan,* **72,** 281–299.

Mo, K. C., and R. W. Higgins, 1996: Large scale atmospheric water vapor transport as evaluated from the NMC/NCAR and the NASA/DAO reanalyses. *J. Climate,* **9,** 1531–1545.

——, J. Nogues-Paegle, and J. Paegle, 1995: Physical mechanisms of the 1993 summer floods. *J. Atmos. Sci.,* **52,** 879–895.

Moorthi, S., and M. J. Suarez, 1992: Relaxed Arakawa–Schubert: A parameterization of moist convection for general circulation models. *Mon. Wea. Rev.,* **120,** 978–1002.

Murakami, T., T. Nakazawa, and J. He, 1984: On the 40–50 day oscillations during the 1979 Northern Hemisphere summer. Part II: Heat and moisture budget. *J. Meteor. Soc. Japan,* **62,** 469–484.

Namias, J., 1982: Anatomy of Great Plains protracted heat waves (especially the 1980 U.S. summer drought). *Mon. Wea. Rev.,* **110,** 824–838.

Paegle, J., 1984: Topographically bound low-level circulations. *Riv. Meteor. Aeronaut.,* **44,** 113–125.

——, and T. Vukicevic, 1987: The analysis and forecast sensitivity of low-level mountain flows to input data. Preprints, *Fourth Conf. on Mountain Meteorology,* Seattle, WA, Amer. Meteor. Soc., 168–174.

Pan, H.-L., and L. Mahrt, 1987: Interaction between soil hydrology and boundary-layer development. *Bound.-Layer Meteor.,* **38,** 185–220.

——, and W.-S. Wu, 1994: Implementing a mass flux convection parameterization package for the NMC medium-range forecast model. Preprints, *10th Conf. on Numerical Weather Prediction,* Portland, OR, Amer. Meteor. Soc., 96–98.

Park, C.-K., S. D. Schubert, D. J. Lamich, and Y. Kondratyeva, 1996: Monsoon rainfall in the GEOS-1 assimilation: Sensitivity to input data. *Proc. 20th Annual Climate Diagnostics Workshop,* Seattle, WA, 61–64.

Parrish, D. F., and J. C. Derber, 1992: The National Meteorological Center's spectral statistical interpolation analysis system. *Mon. Wea. Rev.,* **120,** 1747–1763.

Peixoto, J. P., and A. H. Oort, 1983: The atmospheric branch of the hydrological cycle and climate. *Variations in the Global Water Budget,* A. Street-Perrott et al., Eds., D. Reidel, 5–65.

Pfaendtner, J., S. Bloom, D. Lamich, M. Seablom, M. Sienkiewicz, J. Stobie, and A. da Silva, 1995: Documentation of the Goddard Earth Observing System (GEOS) Data Assimilation System—Version 1. NASA Tech. Memo. 104606, Vol. 4, 44 pp. [Available from Goddard Space Flight Center, Greenbelt, MD 20771.]

Rasmusson, E. M., 1967: Atmospheric water vapor transport and the water balance of North America, Part I. Characteristics of the water vapor flux field. *Mon. Wea. Rev.,* **95,** 403–426.

——, 1968: Atmospheric water vapor transport and the water balance of North America, Part II. Large-scale water balance investigations. *Mon. Wea. Rev.,* **96,** 720–734.

Reynolds, W. R., and D. S. Marsico, 1993: An improved real-time global sea surface temperature analysis. *J. Climate,* **6,** 114–119.

——, and T. M. Smith, 1994: Improved global sea surface temperature analyses using optimum interpolation. *J. Climate,* **7,** 929–948.

Roads, J. O., S.-C. Chen, A. K. Guetter, and K. P. Georgakakos, 1994: Large-scale aspects of the United States hydrological cycle. *Bull. Amer. Meteor. Soc.,* **75,** 1589–1610.

Rosen, R. D., D. A. Salstein, and J. P. Peixoto, 1979: Variability in the annual fields of large-scale atmospheric water vapor transport. *Mon. Wea. Rev.,* **107,** 26–37.

Schemm, J.-K., S. Schubert, J. Terry, and S. Bloom, 1992: Estimates of monthly mean soil moisture for 1979–89. NASA Tech. Memo. 104571, 252 pp. [Available from Goddard Space Flight Center, Greenbelt, MD 20771.]

Schubert, S. D., and R. B. Rood, 1995: Proceedings of the workshop on the GEOS-1 five-year assimilation. NASA Tech. Memo.

104606, Vol. 7, 201 pp. [Available from Goddard Space Flight Center, Greenbelt, MD 20771.]

——, ——, and J. Pfaendtner, 1993: An assimilated dataset for earth science applications. *Bull. Amer. Meteor. Soc.,* **74,** 2331–2342.

——, C.-K, Park, C.-Y. Wu, W. Higgins, Y. Kondratyeva, A. Molod, L. Takacs, M. Seablom, and R. Rood, 1995: A multiyear assimilation with the GEOS-1 system: Overview and results. NASA Tech. Memo. 104606, Vol. 6, 183 pp. [Available from Goddard Space Flight Center, Greenbelt, MD 20771.]

Spencer, R., 1993: Global oceanic precipitation from the MSU during 1979–1991, and comparisons to other climatologies. *J. Climate,* **6,** 1301–1326.

Stensrud, D. J., 1996: Importance of low-level jets to climate: A review. *J. Climate,* **9,** 1698–1711.

Suarez, M. J., and L. L. Takacs, 1995: Documentation of the Aries-GEOS Dynamical Core:Version 2. NASA Tech. Memo. 104606, Vol. 5, 58 pp. [Available from Goddard Space Flight Center, Greenbelt, MD 20771.]

Takacs, L. L., A. Molod, and T. Wang, 1994: Goddard Earth Observing System (GEOS) General Circulation Model (GCM) Version 1. NASA Tech. Memo. 104606, Vol. 1, 100 pp. [Available from Goddard Space Flight Center, Greenbelt, MD 20771.]

Tiedtke, M., 1989: A comprehensive mass flux scheme for cumulus parameterization in large-scale models. *Mon. Wea. Rev.,* **117,** 1777–1798.

Trenberth, K. E., 1991: Climate diagnostics from global analyses: Conservation of mass in ECMWF analyses. *J. Climate,* **4,** 707–722.

——, 1992: Global analyses from ECMWF and atlas of 1000 to 10 mb circulation statistics. NCAR Tech. Note. NCAR/TN-373+STR, 191 pp. plus 24 fiche. [Available from NCAR, Boulder, CO 80307.]

——, 1995: Truncation and use of model-coordinate data. *Tellus,* **47A,** 287–303.

——, and J. G. Olson, 1988: An evaluation and intercomparison of global analyses from the National Meteorological Center and the European Center for Medium Range Weather Forecasts. *Bull. Amer. Meteor. Soc.,* **69,** 1047–1057.

——, and C. J. Guillemot, 1995: Evaluation of the global atmospheric moisture budget as seen from analyses. *J. Climate,* **8,** 2255–2272.

Troen, I., and L. Mahrt, 1986: A simple model of the atmospheric boundary layer: Sensitivity to surface evaporation. *Bound.-Layer Meteor.,* **37,** 129–148.

Wang, M., and J. N. Paegle, 1996: Impact of analysis uncertainty upon regional atmospheric moisture flux. *J. Geophys. Res.,* **101,** 7291–7303.